

This is a copy of the published version, or version of record, available on the publisher's website. This version does not track changes, errata, or withdrawals on the publisher's site.

# Field-induced phase transitions and anisotropic magnetic properties of the Kitaev-Heisenberg compound $\text{Na}_2\text{Co}_2\text{TeO}_6$

A. K. Bera, S. M. Yusuf, F. Orlandi, P. Manuel, L. Bhaskaran, and S. A. Zvyagin





## Published version information

**Citation:** Bera (et.al.) Field-induced phase transitions and anisotropic magnetic properties of the Kitaev-Heisenberg compound  $\text{Na}_2\text{Co}_2\text{TeO}_6$ , Phys. Rev. B 108, 214419


**DOI:** <https://doi.org/10.1103/PhysRevB.108.214419>

This version is made available in accordance with publisher policies. Please cite only the published version using the reference above. This is the citation assigned by the publisher at the time of issuing the APV. Please check the publisher's website for any updates.

## Field-induced phase transitions and anisotropic magnetic properties of the Kitaev-Heisenberg compound $\text{Na}_2\text{Co}_2\text{TeO}_6$

A. K. Bera  and S. M. Yusuf <sup>\*</sup>Solid State Physics Division, Bhabha Atomic Research Centre, Mumbai 400085, India  
and Homi Bhabha National Institute, Anushaktinagar, Mumbai 400094, IndiaF. Orlandi  and P. Manuel 

ISIS Facility, STFC Rutherford Appleton Laboratory, Harwell Oxford, Didcot OX11 0QX, United Kingdom

L. Bhaskaran and S. A. Zvyagin 

Dresden High Magnetic Field Laboratory (HLD-EMFL), Helmholtz-Zentrum Dresden-Rossendorf, 01328 Dresden, Germany



(Received 31 March 2023; revised 18 November 2023; accepted 21 November 2023; published 18 December 2023)

Spin systems with honeycomb structures have recently attracted a great deal of attention in connection with the Kitaev quantum spin liquid state (QSL) predicted theoretically. One possible Kitaev QSL candidate is  $\text{Na}_2\text{Co}_2\text{TeO}_6$  realizing a honeycomb lattice of pseudospin  $1/2$ . Field-dependent single-crystal neutron diffraction technique allows us to determine the microscopic spin-spin correlations across the field-induced phase transitions for  $H \parallel a$  and  $H \parallel a^*$  in plane field directions. Our results reveal phase transitions, initially to a canted zigzag antiferromagnetic state at approximately 60 kOe, followed by a possible transition to a partially polarized state over the range 90–120 kOe, and finally to a field-induced fully polarized state above 120 kOe. We observe distinct field dependencies of the magnetic peak intensities for  $H \parallel a$  and  $H \parallel a^*$ . In addition, low-temperature electron spin resonance in magnetic fields  $H \parallel c$  yields a complete softening for one of the antiferromagnetic resonances at  $\sim 40$  kOe, revealing a field-induced phase transition. The present work thus provides insights into the field evolution of the important Kitaev-Heisenberg spin system  $\text{Na}_2\text{Co}_2\text{TeO}_6$ .

DOI: [10.1103/PhysRevB.108.214419](https://doi.org/10.1103/PhysRevB.108.214419)

### I. INTRODUCTION

The exactly solvable Kitaev honeycomb model [1], based on an effective spin- $1/2$  two-dimensional honeycomb lattice, offers a topological quantum spin liquid (QSL) state with Majorana fermions as excitations. Searching for new materials, where the Kitaev model is realized, is at forefront of modern material science and condensed matter physics. Kitaev interactions or bond-dependent Ising interactions may arise from a spin-orbit entangled pseudospin- $1/2$  degree of freedom in transition metal ions located in edge-shared octahedral crystal fields. A honeycomb-lattice arrangement of such ions is an important prerequisite for the realization of the Kitaev model [2], as it is believed to be the case of  $\text{Na}_2\text{IrO}_3$  [3] and  $\alpha\text{-RuCl}_3$  [4] with the  $d^5$  spin configurations. However, a pure Kitaev material remains elusive due to the presence of additional non-Kitaev interactions, viz., Heisenberg exchange interactions between the pseudospins. Kitaev physics is also predicted for  $d^7$   $\text{Co}^{2+}$  ions with a high-spin  $t_{2g}^5 e_g^2$  configuration that can provide a pseudospin- $1/2$  degree of freedom [5,6]. In this regard, several Co-based candidate Kitaev materials, for instance,  $\text{Na}_2\text{Co}_2\text{TeO}_6$  [7–19],  $\text{BaCo}_2(\text{XO}_4)_2$  ( $X = \text{P}$  and  $\text{As}$ ) [20–22], and  $\text{A}_3\text{Co}_2\text{SbO}_6$  ( $A = \text{Li}, \text{Na}, \text{and Ag}$ ) [12,23,24] have been recently suggested. Among them, the

layered honeycomb magnet  $\text{Na}_2\text{Co}_2\text{TeO}_6$  is of our present interest. Although at low temperature ( $T_N \sim 25$  K)  $\text{Na}_2\text{Co}_2\text{TeO}_6$  orders magnetically [10,11,15,16] (similar to  $\text{Na}_2\text{IrO}_3$  [3] and  $\alpha\text{-RuCl}_3$  [4]), this material has shown some signatures [viz., field-induced disappearance of the peaks observed on specific heat and  $\chi(T)$ , as well as enhancement of magnetic entropy with applied magnetic field] of the Kitaev-Heisenberg physics [12,19].

The crystal structure of  $\text{Na}_2\text{Co}_2\text{TeO}_6$  [Fig. 1(a)] (hexagonal symmetry, space group  $P6_322$ ) is constituted by edge-sharing  $\text{CoO}_6$  and  $\text{TeO}_6$  octahedra that form a perfect honeycomb lattice of  $\text{Co}^{2+}$  ions [Fig. 1(b)]. Such honeycomb layers are running perpendicular to the  $c$  axis, and well separated from each other ( $\sim 5.61$  Å) by intermediate  $\text{Na}^+$  layers. Although the magnetic honeycomb lattice is comprised by two crystallographically independent  $\text{Co}^{2+}$  sites [Wyckoff positions  $2b$  and  $2d$ , respectively], the oxygen octahedra surrounding the sites are similar to the Co-O distances differing by only about 1% [15], resulting in an almost identical environment. Anisotropic Kitaev interactions are predicted to exist between Co ions [5,6] [Fig. 1(b)], in addition to Heisenberg interactions. Most interestingly, similar to  $\text{Na}_2\text{IrO}_3$  and  $\alpha\text{-RuCl}_3$  [4,26–28] a rich temperature-field phase diagram was also reported for  $\text{Na}_2\text{Co}_2\text{TeO}_6$  [11,26–30]. Such phase diagrams are regarded as a characteristic feature of the Heisenberg-Kitaev anisotropic model and reveal the presence of a possible QSL phase in the vicinity of the

<sup>\*</sup>smyusuf@barc.gov.in

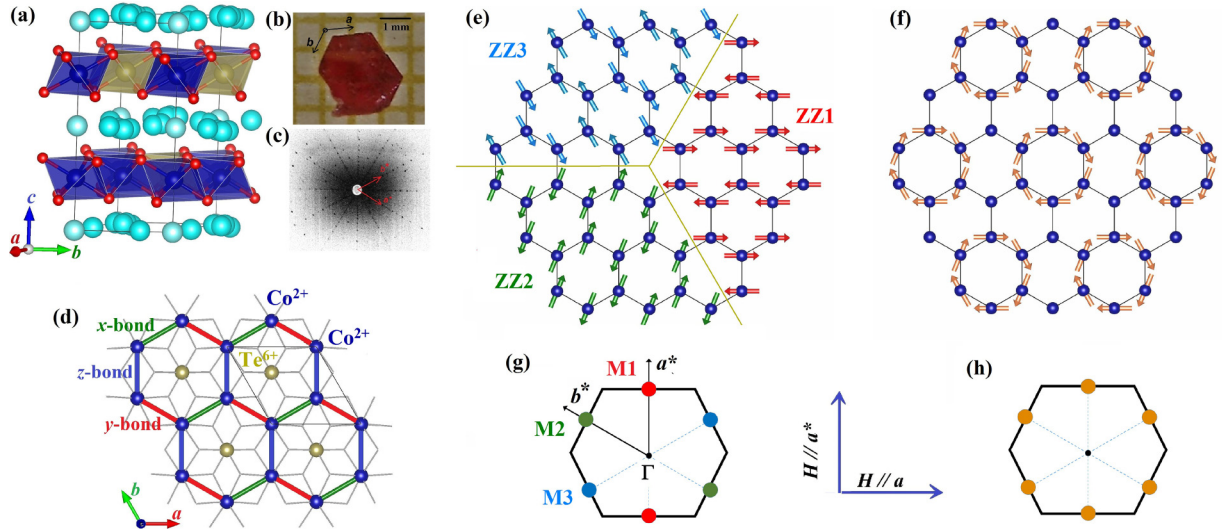


FIG. 1. (a) The layered type crystal structure of  $\text{Na}_2\text{Co}_2\text{TeO}_6$ . (b) Photograph of a representative crystal on a millimeter grid. (c) The x-ray Laue diffraction pattern from the crystal. (d) The in-plane honeycomb layer of  $\text{Co}^{2+}$  ions with the  $\text{Te}^{6+}$  ions in centers of honeycomb cells. Kitaev interactions between the  $x$ ,  $y$ , and  $z$  components of the pseudospins are shown by thick lines with different colors. (e) A schematic of the collinear zigzag magnetic structure and its orientation domains. (f) A schematic of the noncollinear triple- $Q$  magnetic structure. (g),(h) The Bragg peak positions in the first Brillouin zone for the collinear zigzag AFM and noncollinear triple- $Q$  structures, respectively. Magnetic structures were drawn by using VESTA 3 software [25]. The scheme of the applied field directions in the present study is also shown.

quantum critical point [31]. Although the magnetic properties of  $\text{Na}_2\text{Co}_2\text{TeO}_6$  have been recently intensively studied [11,14,17,18,29,30,32–36], the question on the nature of field-induced states (in particular, in regard to the proposed Kitaev QSL) remains open. Several recent studies [17,18,32,36] reported the possible presence of the Kitaev QSL state in the intermediate fields above the field-induced transition at  $H_c$ , however, other studies [11,33,35] suggested the absence of the QSL state.

In this paper, we report results of an extensive neutron diffraction study of high-quality single crystals of  $\text{Na}_2\text{Co}_2\text{TeO}_6$  for in-plane applied magnetic fields with  $H \parallel a$  and  $H \parallel a^*$  directions (for the field direction schemes see Fig. 1), which enable us to reveal the field evolution of its magnetic phases. Magnetic-field-dependent phase diagrams are proposed based on the neutron diffraction results. Furthermore, we report very different behaviors for the field evolutions of the magnetic phases for out-of-plane applied magnetic field ( $H \parallel c$ ) as compared to the in-plane applied magnetic field for the Kitaev-Heisenberg material  $\text{Na}_2\text{Co}_2\text{TeO}_6$ .

## II. EXPERIMENT

Polycrystalline samples of  $\text{Na}_2\text{Co}_2\text{TeO}_6$  were prepared by a solid-state method [15]. High-quality single crystals were grown by a self-flux method [14]. The crystals were characterized by x-ray backscattering Laue diffraction which confirms the sixfold symmetry [Figs. 1(b) and 1(c)] and the good quality of our crystals. The magnetization measurements on single-crystal samples (for applied field along principal axes) were performed with a vibrating sample magnetometer (VSM, Cryogenic Co. Ltd., UK) [Figs. 1(b) and 1(c)]. Temperature-dependent zero-field powder neutron diffraction

measurements and magnetic-field-dependent single-crystal diffraction measurements (for  $H \parallel a$  and  $H \parallel a^*$ ) were performed on the WISH diffractometer at the ISIS facility, RAL, UK [37]. The measured zero-field powder diffraction patterns were analyzed using the Rietveld refinement technique, employing the FULLPROF computer program [38]. High-field ( $H \parallel c$ ) electron spin resonance (ESR) measurements were performed employing a 16 T transmission-type ESR spectrometer (similar to that described in Ref. [39]) in the 100–700-GHz frequency range; the experiments were done in the Faraday configuration.

## III. RESULTS AND DISCUSSION

The single crystals are preliminarily characterized by temperature- and field-dependent magnetization measurements with magnetic field applied along three principal axes  $H \parallel a$ ,  $H \parallel a^*$ , and  $H \parallel c$  (see Fig. S1 in the Supplemental Material [40]), which reveal that the magnetism in  $\text{Na}_2\text{Co}_2\text{TeO}_6$  is highly anisotropic and close to tipping points between competing phases. The observed results have been used to draw the phase diagrams (Fig. S1, Supplemental Material [40]), which reveal field-induced transitions at  $\sim 60$  kOe for both  $H \parallel a$  and  $H \parallel a^*$ . The field-induced phases are proposed to host the Kitaev QSL state. The above results are in good agreement with that reported earlier [11]. In the present study, we employed field-dependent single-crystal neutron diffraction to determine the field evolution of the magnetic phases at 1.5 K (the experimental geometry is shown in Fig. 1). Before, presenting the results of our field-dependent single-crystal neutron diffraction study, we first describe below the magnetic ground state (in zero magnetic field) of the compound. The magnetic ground state of  $\text{Na}_2\text{Co}_2\text{TeO}_6$  was initially reported to be a zigzag based collinear

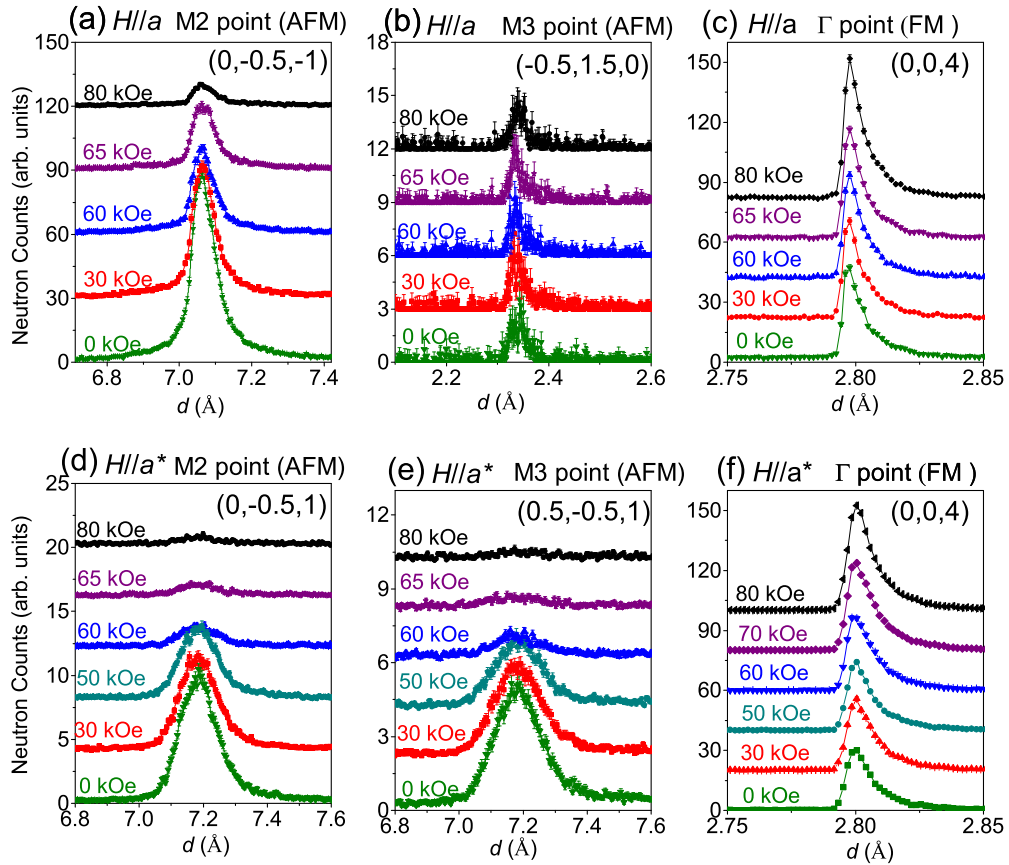


FIG. 2. The field evolution of representative magnetic Bragg peaks at the  $M2$ ,  $M3$ , and  $\Gamma$  points of the BZ for (a)–(c)  $H \parallel a$  and (d)–(f)  $H \parallel a^*$ , respectively. The measured diffraction patterns are offset vertically for clarity. The asymmetric peak shapes, especially for low- $d$  value Bragg peaks, appear due to intrinsic feature of the time-of-flight diffractometer. Here, the moderation process generates pulses of neutron that, at a fixed wavelength, have a characteristic back-to-back exponential profile which in turn is responsible for the peak shape of the Bragg reflections.

antiferromagnetic (AFM) structure by neutron powder diffraction [15,16]. The long-range zigzag AFM ordering [with propagation vector  $\mathbf{k} = (1/2, 0, 0)$ ] [15] manifests itself as sharp magnetic Bragg peaks at the  $M$  points of the Brillouin zone (BZ) in the  $(H, K, 0)$  plane. As the zigzag AFM order breaks the threefold rotation symmetry ( $C3$ ) of the hexagonal lattice, three magnetic domains (differing by an angle of  $120^\circ$ ) are present [26]. Therefore, in the zigzag AFM phase [9,15,16], one should expect a total of six peaks [Fig. 1(g)] at six  $M$  points [represented by the propagation vectors  $\mathbf{k}_1 = (\frac{1}{2}00)$ ,  $\mathbf{k}_2 = (0\frac{1}{2}0)$ , and  $\mathbf{k}_3 = (\frac{1}{2}-\frac{1}{2}0)$ , respectively] from the three magnetic domains. However, based on recent elastic and inelastic neutron scattering studies on single-crystal samples as well as theoretical modeling on  $\text{Na}_2\text{Co}_2\text{TeO}_6$  [9,41,42], it has been established that a “triple- $Q$ ” magnetic state [Fig. 1(f)] is the most appropriate one. It is important to add here that the Bragg-peak pattern of a single magnetic domain of a triple- $Q$  state (consisting of six sharp peaks at all the  $M$  points [Fig. 1(h)]), is identical to the averaged pattern of three domains of the single- $Q$  zigzag AFM state. Therefore, the triple- $Q$  and zigzag orders cannot be distinguished by neutron diffraction [9], unless the populations of the domains become unequal by external perturbations like magnetic field [41], strain, and/or pressure, i.e., by the

breaking of the hexagonal  $C3$  symmetry. Besides, a recent study on  $\text{Na}_2\text{Co}_2\text{TeO}_6$  using muon spin relaxation [43] reveals the presence of prevalent spin dynamics with spatially uneven distribution and varied correlation times as well. The muon spin relaxation results imply that the magnetic ground state of  $\text{Na}_2\text{Co}_2\text{TeO}_6$  cannot be solely described by the long-range triple- $Q$  static order, suggesting a significant role of quantum fluctuations in establishing its ground state.

The field-induced evolution of the magnetic state is investigated directly by measuring the variations of magnetic Bragg peak intensities at the  $M$  points in the BZ as well as nuclear Bragg peaks at the  $\Gamma$  point of the BZ as a function of applied magnetic field for both applied field directions  $H \parallel a$  and  $H \parallel a^*$  [Figs. 2(a)–2(f)]. The corresponding variations of the integrated intensities are shown in Figs. 3(a)–3(f), indicating anomalies at critical fields for both  $H \parallel a$  and  $H \parallel a^*$ . For the applied field along  $H \parallel a$ , the intensities of all magnetic Bragg peaks [(0, -0.5, 0), (0, -0.5, -1), (0, -0.5, -2), and (0, -0.5, -3)] corresponding to the  $M2$  reciprocal points decrease linearly with the increasing field up to  $H_{c1} = 60$  kOe and attain  $\sim 40 - 60\%$  of their corresponding zero-field intensities [Fig. 3(a)]. Above  $H_{c1}$ , a linear decrease of the intensities is also evident. The slope ( $dI/dH$ ) is higher for  $H > H_{c1}$  than that for  $H < H_{c1}$  [Fig. 3(a)]. The change of slope occurs

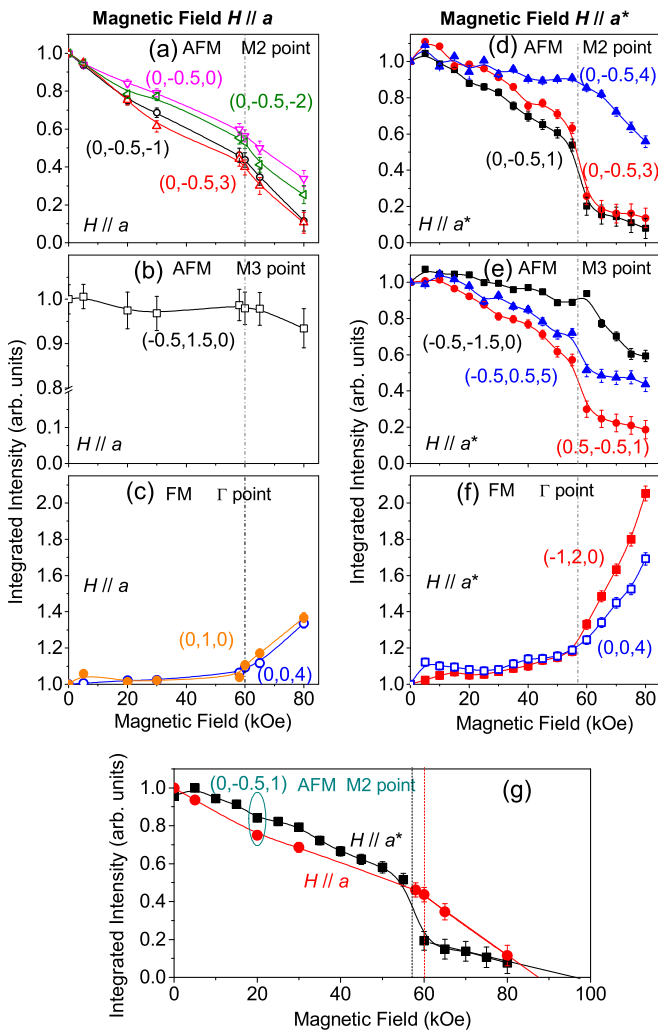


FIG. 3. (a)–(c) The field evolution of the integrated intensity of magnetic Bragg peaks of  $\text{Na}_2\text{Co}_2\text{TeO}_6$  at  $M2$ ,  $M3$ , and  $\Gamma$  points of the BZ under the magnetic fields for (a)–(c)  $H \parallel a$  and (d)–(f)  $H \parallel a^*$ , respectively. All the intensities of the magnetic Bragg peaks are normalized with respect to their zero field values. (g) A comparison between the field dependence of the intensity of the AFM peak at  $M2$  point for  $H \parallel a$  and  $H \parallel a^*$ .

at  $H_{c1}$ , in line with the bulk magnetization (Fig. S1) in the Supplemental Material [40]. A similar behavior has also been found for the magnetic Bragg peak at the  $M3$  point [Fig. 3(b)] of the second BZ. It may be noted here that the variation of the intensity for the magnetic Bragg peaks with  $L = \text{odd}$  indices is slightly larger than that for the  $L = \text{even}$  case. Due to the instrumental geometry with the vertical magnetic field, no magnetic Bragg peaks corresponding to the  $M1$  point of the BZ are accessible. In addition, we have shown the intensity variation of the selective nuclear Bragg peaks at the  $\Gamma$  point [Fig. 3(c)]. An enhancement of the intensities of the nuclear Bragg peaks  $(0, 0, 4)$  and  $(0, 1, 0)$  is found with increasing magnetic field. The additional magnetic signal at these nuclear Bragg peak points is, therefore, due to a field-induced uniform magnetization. This means that the suppression of the antiferromagnetic order is due to the significant spin polarization along the applied magnetic field  $H \parallel a$ . However, the

maximum applied field of 80 kOe is not sufficient to achieve the complete parallel alignment of the moments as also indicated by the bulk magnetization data. This implies that the system is in a magnetically ordered state under applied field  $H \parallel a$  up to 80 kOe, and the expected field-induced spin liquid state is not yet achieved (discussed in detail later).

Now, we present additional data for the in-plane applied field direction  $H \parallel a^*$ . The variation of the intensity of the magnetic peaks with the applied magnetic field reveals a completely different behavior than that for the  $H \parallel a$ . With the increasing field for  $H \parallel a^*$ , the intensities of the magnetic Bragg peaks at  $M2$  and  $M3$  points are enhanced slightly for  $H$  up to  $\sim 5$  kOe, and then decrease linearly over  $5 < H < 57$  kOe ( $H_{c1}$ ) [Figs. 3(d) and 3(e)]. However, at  $H = H_{c1}$ , the intensities of the magnetic Bragg peaks with  $L = \text{odd}$  indices [i.e.,  $(0, -0.5, 1)$ ,  $(0, -0.5, 3)$ ,  $(0.5, -0.5, 1)$ , and  $(0.5, -0.5, 5)$ ] fall sharply by  $\sim 40\%$ , and attain  $\sim 20\%$  of their zero field values. The observed sharp fall is in contrast to the results for  $H \parallel a$ , presented in the previous section. Nevertheless, they are in line with the observed first-order field-induced transition of magnetization (Fig. S1). In contrast, no sharp drop in intensity at the  $H_{c1}$  is observed for the magnetic Bragg peak with  $L = \text{even}$  indices [i.e.,  $(0, -0.5, 4)$  and  $(-0.5, -1.5, 0)$ ], rather only a change in slope ( $dI/dH$ ) is evident at  $H_{c1}$  (as in the case for  $H \parallel a$ ). Upon further increasing the magnetic field above  $H_{c1}$ , the intensities decrease linearly. The residual intensity of the magnetic Bragg peak  $(0, -0.5, 4)$  with  $L = \text{even}$  is found to be  $\sim 50\%$  of the zero field intensity at 80 kOe as compared to  $\sim 10\%$  for the magnetic peaks with  $L = \text{odd}$  indices [i.e.,  $(0, -0.5, 1)$  and  $(0, -0.5, 3)$ ]. Such contrasting behaviors for the planes with  $L = \text{odd}$  and  $L = \text{even}$  are unique and have been revealed by the present comprehensive single-crystal neutron diffraction study. This is consistent with the antiferromagnetically coupling of the magnetic planes having triple- $Q$  structure along the  $c$  axis in  $\text{Na}_2\text{Co}_2\text{TeO}_6$  [15] and reveals a different chirality for the alternating magnetic planes along the  $c$  axis. For this field configuration as well, an enhancement of the intensities of the nuclear Bragg peaks  $(0, 0, 4)$  and  $(-1, 2, 0)$  are found with increasing magnetic field [Fig. 3(f)]. However, the relative change of the intensity is much stronger as compared to the same for  $H \parallel a$ . As the neutron diffraction is only sensitive to the ordered moment component perpendicular to the wave-vector transfer  $\mathbf{Q}$ , the enhancement of the intensity of the  $(0, 0, 4)$  nuclear Bragg peak suggests that the ferromagnetic (FM) component lies mainly within the  $ab$  plane. The in-plane FM component is also evident from the higher bulk magnetization values for the in-plane fields ( $H \parallel a$  and  $H \parallel a^*$ ) as compared to that for the  $H \parallel c$  (Fig. S1 in the Supplemental Material [40]). Further, the enhancement of the intensities of the Bragg peaks  $(-1, 2, 0)$  for  $H \parallel a^*$  reveals that the FM moments develop along the applied field directions. Therefore, the additional magnetic signal of the nuclear Bragg peaks is due to field-induced uniform magnetization as in the case for  $H \parallel a$ . The intensities of the AFM Bragg peaks persist ( $\sim 20 - 40\%$  of their corresponding intensities in the zero field) up to 80 kOe for  $H \parallel a^*$  revealing the presence of the magnetically ordered state. This also implies that the spin liquid state is not achieved even up to a field of 80 kOe for  $H \parallel a^*$  as well (discussed in detail later). Nevertheless, our results

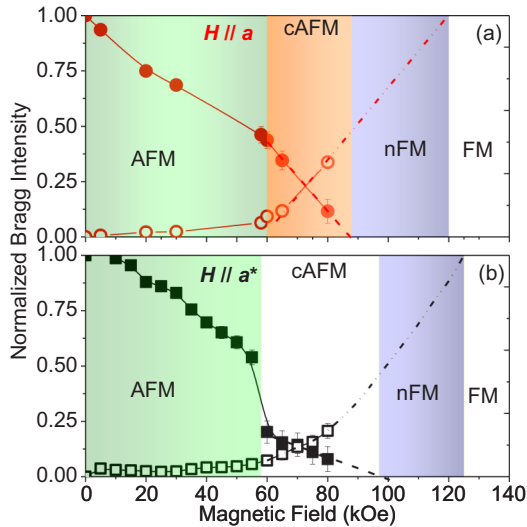


FIG. 4. The magnetic phase diagrams of  $\text{Na}_2\text{Co}_2\text{TeO}_6$  at 1.5 K for (a)  $H \parallel a$  and (b)  $H \parallel a^*$ , respectively. The AFM, cAFM, nFM, and FM stand for antiferromagnetic, canted antiferromagnetic, near field polarization, and field polarized states, respectively.

unambiguously reveal different field dependencies for the  $H \parallel a$  and  $H \parallel a^*$  directions especially around the critical magnetic field  $H_{c1}$  as evident from the direct comparison of the field dependence for the  $M2$  (0, -0.5, 1) point [Fig. 3(g)]. Such a different field dependence is unusual considering the  $C3$  symmetry of the recently proposed triple- $Q$  magnetic ground state.

The observed variations of the normalized intensity of the AFM and FM components from the present single-crystal neutron diffraction study at 1.5 K are fruitfully used to draw the field-dependent magnetic phase diagrams for  $H \parallel a$  and  $H \parallel a^*$  (Fig. 4). For the AFM Bragg phase, the peaks intensity is normalized to the zero-field intensity. The intensity of the nuclear Bragg peak (0, 0, 4) is normalized with the intensity expected for the completely polarized (FM) state with the magnetic moment along the  $a$  and  $a^*$  axes corresponding to the cases for  $H \parallel a$  [Fig. 3(c)] and  $H \parallel a^*$  [Fig. 3(f)], respectively. The linear extrapolation of the AFM intensity reveals that it persists up to  $H_{c2} \sim 90$  and 95 kOe for the applied fields  $H \parallel a$  and  $H \parallel a^*$ , respectively (Fig. 4). On the other hand, the extrapolation of the FM intensity reveals that the full polarization occurs only above  $H_S \sim 120$  and 125 kOe for the applied fields  $H \parallel a$  and  $H \parallel a^*$ , respectively. This agrees with the bulk magnetization where a near saturation is achieved above  $\sim 120$  kOe. In agreement with our results, recent magnetic phase diagrams have been proposed for  $\text{Na}_2\text{Co}_2\text{TeO}_6$  under in-plane applied fields, suggesting the existence of two field-induced intermediate states (prior to reaching the field-polarized state) [44]. The magnetic phases between the  $H_{c1}$  and  $H_{c2}$ , where the coexistence of both the AFM and FM Bragg peaks are observed, can be labeled as canted antiferromagnetic (cAFM). Recent theoretical study predicts a metamagnetic phase transition (in the classical limit) from the triple- $Q$  ground state to a canted zigzag state ( $z$  zigzag for  $H \parallel a^*$  and  $x/y$  zigzag for  $H \parallel a$ ) at intermediate fields, preceding the transition toward the field-induced polarized state at higher

fields [42]. A comparison of the measured intensities (Fig. 3) for both the field directions with the simulated magnetic Bragg peak intensities (considering such cAFM structures with the moment components for 80 kOe) gives a satisfactory agreement [Figs. S5(a) and S5(b) in the Supplemental Material [40]]. Further analysis of our single-crystal data (Fig. S6 in the Supplemental Material [40]) rules out the presence of any additional field-induced ordered state (as reported for the most extensively studied Kitaev-Heisenberg model compound  $\alpha\text{-RuCl}_3$  and labeled as the second zigzag AFM phase, ZZ2 state) [45]) over this intermediate field range. Moreover, the phase diagrams show that only a partial polarized (FM) phase is present over the field region  $H_{c2} - H_S$ .

Our recent high-resolution terahertz spectroscopy study on  $\text{Na}_2\text{Co}_2\text{TeO}_6$  as a function of applied magnetic field with different terahertz polarizations [46] illustrate spin dynamics with distinct characteristics over magnetic field 0–70 kOe, 70–100 kOe, and above 100 kOe. While below 70 kOe and above 100 kOe the dynamics is characterized by well-defined magnetic excitations, in the intermediate regime 70–100 kOe reveals a sharp absorption profile and extended continuum in the longitudinal and transverse polarization channels for both the applied field directions  $H \parallel a$  and  $H \parallel a^*$ . A polarization-selective continuum in the intermediate phase is an indication for spin fluctuations of a proximate quantum spin liquid. Furthermore, recent experimental studies of  $\text{Na}_2\text{Co}_2\text{TeO}_6$  employing various techniques, such as magnetic torque [29], specific heat [17], thermal transport [18,33], have unveiled intriguing properties under in-plane fields above the critical field. These observations imply that the field-induced near-polarized states exhibit characteristics distinct from those of a conventional paramagnet. Additionally, a recent theoretical study has reported a field-induced transition from the low-field ordered state to a gapless quantum spin liquid at intermediate fields, occurring prior to the emergence of the field-induced polarized state [47].

Now we shed light on the nature of the field-dependent state for  $H \parallel c$  by field and temperature-dependent electron spin resonance (ESR) measurements on the  $\text{Na}_2\text{Co}_2\text{TeO}_6$  single crystals. The ESR spectra measured at 2 K for  $H \parallel c$  [Fig. 5(a)] reveal three modes of antiferromagnetic resonance (AFMR)  $A$ ,  $B$ , and  $C$ , respectively. The extrapolation of the frequency-field dependencies of the observed excitations to zero field suggests the presence of the energy gap,  $\Delta = 240$  GHz ( $\sim 1$  meV), which is similar to that observed previously by inelastic neutron scattering [30,48]. The modes  $A$  and  $B$  demonstrate linear increase in the resonance-frequency position, while mode  $C$  exhibits softening with increasing field. The extrapolation of the  $C$  mode suggests a complete softening at  $\sim 40$  kOe where a change in slope in the  $M$  vs  $H$  curve as well as a change in the nature of the susceptibility curves is found (Fig. S1 in the Supplemental Material [40]). The above experimental observation might be an indication of a field-induced phase transition at 40 kOe. Upon increasing the temperature, the AFMR modes  $A$  and  $B$  become broader and cannot be resolved anymore at or above  $T_N = 27$  K (Fig. 5). The mode  $C$  exhibits a substantial broadening at low frequencies, suggesting the presence of two resonance lines (AFMR modes  $C$  and  $C'$ ), similar to that revealed for the higher-frequency absorptions (AFMR modes  $A$  and  $B$ ). The

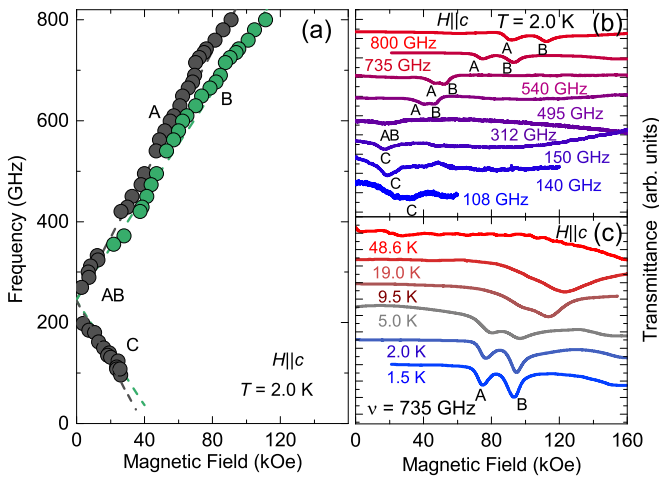


FIG. 5. (a) Frequency-field dependencies of ESR excitations measured at  $T = 2.0$  K with magnetic field applied along the  $c$  axis. The dashed lines are guides to the eyes. (b) Examples of ESR spectra taken at  $T = 2.0$  K. (c) ESR spectra measured at a frequency of 735 GHz and different temperatures. The spectra in (b) and (c) are offset vertically for clarity.

presence of this double-peak structure of the ESR absorptions can be explained taking into consideration possible tiny twinning of the crystal along the  $c$  axis.

#### IV. CONCLUSION

In conclusion, we have presented results of single-crystal static magnetic susceptibility, neutron diffraction, and ESR studies along with powder heat capacity of  $\text{Na}_2\text{Co}_2\text{TeO}_6$ , allowing us to shed light on the microscopic nature of the field-induced phases. Our comprehensive study under applied magnetic field along  $H \parallel a$ ,  $H \parallel a^*$ , and  $H \parallel c$  determines the

field evolution of the magnetic phases. Our findings reveal that phase transitions occur from the ordered ground state to an ordered canted zigzag antiferromagnetic state at approximately 60 kOe, followed by a possible transition to a partially polarized state (over the range of approximately 90–120 kOe), and ultimately to a field-induced fully polarized state (above approximately 120 kOe). Notably, our results also highlight the distinct field dependencies of the magnetic peak intensities for in-plane field directions  $H \parallel a$  and  $H \parallel a^*$ . These field-induced near-polarization states exhibit distinct characteristics and warrant further investigation to unveil their exotic magnetism. Conversely, for  $H \parallel c$ , we have identified a phase transition at 40 kOe through field and temperature-dependent electron spin resonance (ESR) measurements.

Data are available from the authors under reasonable request.

#### ACKNOWLEDGMENTS

A.K.B. and S.M.Y. thank the Department of Science and Technology, India (Grant No. SR/NM/Z-07/2015) for the access to the experimental facility and financial support to carry out the neutron scattering experiment, and Jawaharlal Nehru Centre for Advanced Scientific Research (JNCASR) for managing the project. The authors thank the Science and Technology Facilities Council (UK) for the provision of neutron beam time on the WISH beam line [49]. For the purpose of open access, the author has applied a creative commons attribution (CC BY) license to any author accepted manuscript version arising. This work was supported by the Deutsche Forschungsgemeinschaft and SFB 1143, as well as by HLD at HZDR, member of the European Magnetic Field Laboratory (EMFL).

- [1] A. Kitaev, Anyons in an exactly solved model and beyond, *Ann. Phys.* **321**, 2 (2006).
- [2] H. Takagi, T. Takayama, G. Jackeli, G. Khaliullin, and S. E. Nagler, Concept and realization of Kitaev quantum spin liquids, *Nat. Rev. Phys.* **1**, 264 (2019).
- [3] S. Hwan Chun, J.-W. Kim, J. Kim, H. Zheng, C. C. Stoumpos, C. D. Malliakas, J. F. Mitchell, K. Mehlawat, Y. Singh, Y. Choi, T. Gog, A. Al-Zein, M. M. Sala, M. Krisch, J. Chaloupka, G. Jackeli, G. Khaliullin, and B. J. Kim, Direct evidence for dominant bond-directional interactions in a honeycomb lattice iridate  $\text{Na}_2\text{IrO}_3$ , *Nat. Phys.* **11**, 462 (2015).
- [4] A. Banerjee, M. D. Lumsden, Y. Yiu, J. Knolle, S. Bhattacharjee, D. L. Kovrizhin, R. Moessner, D. A. Tennant, D. G. Mandrus, S. E. Nagler, C. A. Bridges, J.-Q. Yan, A. A. Aczel, L. Li, M. B. Stone, and G. E. Granroth, Proximate Kitaev quantum spin liquid behaviour in a honeycomb magnet, *Nat. Mater.* **15**, 733 (2016).
- [5] H. Liu and G. Khaliullin, Pseudospin exchange interactions in  $d^7$  cobalt compounds: Possible realization of the Kitaev model, *Phys. Rev. B* **97**, 014407 (2018).
- [6] H. Liu, J. r. Chaloupka, and G. Khaliullin, Kitaev spin liquid in 3d transition metal compounds, *Phys. Rev. Lett.* **125**, 047201 (2020).
- [7] C. H. Lee, S. Lee, Y. S. Choi, Z. H. Jang, R. Kalaivanan, R. Sankar, and K.-Y. Choi, Multistage development of anisotropic magnetic correlations in the Co-based honeycomb lattice  $\text{Na}_2\text{Co}_2\text{TeO}_6$ , *Phys. Rev. B* **103**, 214447 (2021).
- [8] C. Kim, H.-S. Kim, and J.-G. Park, Spin-orbital entangled state and realization of Kitaev physics in 3 compounds: a progress report, *J. Phys.: Condens. Matter* **34**, 023001 (2022).
- [9] W. Chen, X. Li, Z. Hu, Z. Hu, L. Yue, R. Sutarto, F. He, K. Iida, K. Kamazawa, W. Yu, X. Lin, and Y. Li, Spin-orbit phase behavior of  $\text{Na}_2\text{Co}_2\text{TeO}_6$  at low temperatures, *Phys. Rev. B* **103**, L180404 (2021).
- [10] A. M. Samarakoon, Q. Chen, H. Zhou, and V. O. Garlea, Static and dynamic magnetic properties of honeycomb lattice antiferromagnets  $\text{Na}_2M_2\text{TeO}_6$ ,  $M = \text{Co}$  and  $\text{Ni}$ , *Phys. Rev. B* **104**, 184415 (2021).

- [11] W. Yao and Y. Li, Ferrimagnetism and anisotropic phase tunability by magnetic fields in  $\text{Na}_2\text{Co}_2\text{TeO}_6$ , *Phys. Rev. B* **101**, 085120 (2020).
- [12] M. Songvilay, J. Robert, S. Petit, J. A. Rodríguez-Rivera, W. D. Ratcliff, F. Damay, V. Balédent, M. Jiménez-Ruiz, P. Lejay, E. Pachoud, A. Hadj-Azzem, V. Simonet, and C. Stock, Kitaev interactions in the Co honeycomb antiferromagnets  $\text{Na}_3\text{Co}_2\text{SbO}_6$  and  $\text{Na}_2\text{Co}_2\text{TeO}_6$ , *Phys. Rev. B* **102**, 224429 (2020).
- [13] Y. Mao and Y. Li, Theoretical study on the anomalies of the magnetic susceptibility in the honeycomb lattice compound  $\text{Na}_2\text{Co}_2\text{TeO}_6$ , *Phys. Rev. B* **102**, 054414 (2020).
- [14] G. Xiao, Z. Xia, W. Zhang, X. Yue, S. Huang, X. Zhang, F. Yang, Y. Song, M. Wei, H. Deng, and D. Jiang, Crystal growth and the magnetic properties of  $\text{Na}_2\text{Co}_2\text{TeO}_6$  with quasi-two-dimensional honeycomb lattice, *Cryst. Growth Des.* **19**, 2658 (2019).
- [15] A. K. Bera, S. M. Yusuf, A. Kumar, and C. Ritter, Zigzag antiferromagnetic ground state with anisotropic correlation lengths in the quasi-two-dimensional honeycomb lattice compound  $\text{Na}_2\text{Co}_2\text{TeO}_6$ , *Phys. Rev. B* **95**, 094424 (2017).
- [16] E. Lefrançois, M. Songvilay, J. Robert, G. Nataf, E. Jordan, L. Chaix, C. V. Colin, P. Lejay, A. Hadj-Azzem, R. Ballou, and V. Simonet, Magnetic properties of the honeycomb oxide  $\text{Na}_2\text{Co}_2\text{TeO}_6$ , *Phys. Rev. B* **94**, 214416 (2016).
- [17] G. Lin, J. Jeong, C. Kim, Y. Wang, Q. Huang, T. Masuda, S. Asai, S. Itoh, G. Günther, M. Russina, Z. Lu, J. Sheng, L. Wang, J. Wang, G. Wang, Q. Ren, C. Xi, W. Tong, L. Ling, Z. Liu *et al.*, Field-induced quantum spin disordered state in spin-1/2 honeycomb magnet  $\text{Na}_2\text{Co}_2\text{TeO}_6$ , *Nat. Commun.* **12**, 5559 (2021).
- [18] X. Hong, M. Gillig, R. Hentrich, W. Yao, V. Kocsis, A. R. Witte, T. Schreiner, D. Baumann, N. Pérez, A. U. B. Wolter, Y. Li, B. Büchner, and C. Hess, Strongly scattered phonon heat transport of the candidate Kitaev material  $\text{Na}_2\text{Co}_2\text{TeO}_6$ , *Phys. Rev. B* **104**, 144426 (2021).
- [19] C. Kim, J. Jeong, G. Lin, P. Park, T. Masuda, S. Asai, S. Itoh, H.-S. Kim, H. Zhou, J. Ma, and J.-G. Park, Antiferromagnetic Kitaev interaction in  $J_{\text{eff}} = 1/2$  cobalt honeycomb materials  $\text{Na}_3\text{Co}_2\text{SbO}_6$  and  $\text{Na}_2\text{Co}_2\text{TeO}_6$ , *J. Phys.: Condens. Matter* **34**, 045802 (2022).
- [20] R. Zhong, T. Gao, N. P. Ong, and R. J. Cava, Weak-field induced nonmagnetic state in a Co-based honeycomb, *Sci. Adv.* **6**, eaay6953 (2020).
- [21] H. S. Nair, J. M. Brown, E. Coldren, G. Hester, M. P. Gelfand, A. Podlesnyak, Q. Huang, and K. A. Ross, Short-range order in the quantum XXZ honeycomb lattice material  $\text{BaCo}_2(\text{PO}_4)_2$ , *Phys. Rev. B* **97**, 134409 (2018).
- [22] P. A. Maksimov, A. V. Ushakov, Z. V. Pchelkina, Y. Li, S. M. Winter, and S. V. Streltsov, Ab initio guided minimal model for the “Kitaev” material  $\text{BaCo}_2(\text{AsO}_4)_2$ : Importance of direct hopping, third-neighbor exchange and quantum fluctuation, *Phys. Rev. B* **106**, 165131 (2022).
- [23] X. Li, Y. Gu, Y. Chen, V. O. Garlea, K. Iida, K. Kamazawa, Y. Li, G. Deng, Q. Xiao, X. Zheng, Z. Ye, Y. Peng, A. Zaliznyak, J. M. Tranquada, and Y. Li, Giant magnetic in-plane anisotropy and competing instabilities in  $\text{Na}_3\text{Co}_2\text{SbO}_6$ , *Phys. Rev. X* **12**, 041024 (2022).
- [24] Q. Duan, H. Bu, V. Pomjakushin, H. Luetkens, Y. Li, J. Zhao, J. S. Gardner, and H. Guo, Anomalous ferromagnetic behavior in orthorhombic  $\text{Li}_3\text{Co}_2\text{SbO}_6$ , *Inorg. Chem.* **61**, 10880 (2022).
- [25] K. Momma and F. Izumi, VESTA 3 for three-dimensional visualization of crystal, volumetric and morphology data, *J. Appl. Crystallogr.* **44**, 1272 (2011).
- [26] J. A. Sears, Y. Zhao, Z. Xu, J. W. Lynn, and Y.-J. Kim, Phase diagram of  $\alpha\text{-RuCl}_3$  in an in-plane magnetic field, *Phys. Rev. B* **95**, 180411(R) (2017).
- [27] A. Banerjee, P. Lampen-Kelley, J. Knolle, C. Balz, A. A. Aczel, B. Winn, Y. Liu, D. Pajerowski, J. Yan, C. A. Bridges, A. T. Savici, B. C. Chakoumakos, M. D. Lumsden, D. A. Tennant, R. Moessner, D. G. Mandrus, and S. E. Nagler, Excitations in the field-induced quantum spin liquid state of  $\alpha\text{-RuCl}_3$ , *npj Quantum Mater.* **3**, 8 (2018).
- [28] R. D. Johnson, S. C. Williams, A. A. Haghighirad, J. Singleton, V. Zapf, P. Manuel, I. I. Mazin, Y. Li, H. O. Jeschke, R. Valentí, and R. Coldea, Monoclinic crystal structure of  $\alpha\text{-RuCl}_3$  and the zigzag antiferromagnetic ground state, *Phys. Rev. B* **92**, 235119 (2015).
- [29] G. Lin, Q. Zhao, G. Li, M. Shu, Y. Ma, J. Jiao, Q. Huang, J. Sheng, A. I. Kolesnikov, L. Li, L. Wu, X. Wang, H. Zhou, Z. Liu, and J. Ma, Evidence for field induced quantum spin liquid behavior in a spin-1/2 honeycomb magnet, *Res. Square* (2022).
- [30] G. Xiao, Z. Xia, Y. Song, and L. Xiao, Magnetic properties and phase diagram of quasi-two-dimensional  $\text{Na}_2\text{Co}_2\text{TeO}_6$  single crystal under high magnetic field, *J. Phys.: Condens. Matter* **34**, 075801 (2021).
- [31] L. Janssen and M. Vojta, Heisenberg–Kitaev physics in magnetic fields, *J. Phys.: Condens. Matter* **31**, 423002 (2019).
- [32] H. Yang, C. Kim, Y. Choi, J. H. Lee, G. Lin, J. Ma, M. Kratochvílová, P. Proschek, E.-G. Moon, K. H. Lee, Y. S. Oh, and J.-G. Park, Significant thermal Hall effect in the 3d cobalt Kitaev system  $\text{Na}_2\text{Co}_2\text{TeO}_6$ , *Phys. Rev. B* **106**, L081116 (2022).
- [33] H. Takeda, J. Mai, M. Akazawa, K. Tamura, J. Yan, K. Moovendaran, K. Raju, R. Sankar, K.-Y. Choi, and M. Yamashita, Planar thermal Hall effects in Kitaev spin liquid candidate  $\text{Na}_2\text{Co}_2\text{TeO}_6$ , *Phys. Rev. Res.* **4**, L042035 (2022).
- [34] S. Mukherjee, G. Manna, P. Saha, S. Majumdar, and S. Giri, Ferroelectric order with a linear high-field magnetoelectric coupling in  $\text{Na}_2\text{Co}_2\text{TeO}_6$ : A proposed Kitaev compound, *Phys. Rev. Mater.* **6**, 054407 (2022).
- [35] J. Kikuchi, T. Kamoda, N. Mera, Y. Takahashi, K. Okumura, and Y. Yasui, Field evolution of magnetic phases and spin dynamics in the honeycomb lattice magnet  $\text{Na}_2\text{Co}_2\text{TeO}_6$ :  $^{23}\text{Na}$  NMR study, *Phys. Rev. B* **106**, 224416 (2022).
- [36] S. K. Guang, N. Li, R. L. Luo, Q. Huang, Y. Y. Wang, X. Y. Yue, K. Xia, Q. J. L. X. Zhao, G. Chen, H. D. Zhou, and X. F. Sun, Thermal transport of fractionalized antiferromagnetic and field induced states in the Kitaev material  $\text{Na}_2\text{Co}_2\text{TeO}_6$ , *Phys. Rev. B* **107**, 184423 (2023).
- [37] L. C. Chapon, P. Manuel, P. G. Radaelli, C. Benson, L. Perrott, S. Ansell, N. J. Rhodes, D. Raspino, D. Duxbury, E. Spill, and J. Norris, Wish: the new powder and single crystal magnetic diffractometer on the second target station, *Neutron News* **22**, 22 (2011).
- [38] J. Rodríguez-Carvajal, Recent advances in magnetic structure determination by neutron powder diffraction, *Phys. B (Amsterdam, Neth.)* **192**, 55 (1993).



- [39] S. A. Zvyagin, J. Krzystek, P. H. M. van Loosdrecht, G. Dhalenne, and A. Revcolevschi, High-field ESR study of the dimerized-incommensurate phase transition in the spin-Peierls compound  $\text{CuGeO}_3$ , *Phys. B (Amsterdam, Neth.)* **346–347**, 1 (2004).
- [40] See Supplemental Material at <http://link.aps.org/supplemental/10.1103/PhysRevB.108.214419> for details on Bulk magnetization and H-T phase diagram, field-dependent specific heat, temperature-dependent zero-field neutron powder diffraction, comparison of experimental and calculated intensities in the canted AFM state, and field-dependent neutron diffraction patterns at the M and  $\Gamma$  point; contains Refs. [7,11,15–17].
- [41] W. Yao, Y. Zhao, Y. Qiu, C. Balz, J. R. Stewart, Jeffrey W. Lynn, and Y. Li, Magnetic ground state of the Kitaev  $\text{Na}_2\text{Co}_2\text{TeO}_6$  spin liquid candidate, *Phys. Rev. Res.* **5**, L022045 (2023).
- [42] W. G. F. Krüger, W. Chen, X. Jin, Y. Li, and L. Janssen, Triple-q Order in  $\text{Na}_2\text{Co}_2\text{TeO}_6$  from proximity to hidden-SU(2)-symmetric point, *Phys. Rev. Lett.* **131**, 146702 (2023).
- [43] P. Miao, X. Jin, W. Yao, Y. Chen, A. Koda, Z. Tan, W. Xie, W. Ji, T. Kamiyama, and Y. Li, Persistent spin dynamics in magnetically ordered honeycomb cobalt oxides, [arXiv:2307.16451](https://arxiv.org/abs/2307.16451).
- [44] S. Zhang, S. Lee, A. J. Woods, W. K. Peria, S. M. Thomas, R. Movshovich, E. Brosha, Q. Huang, H. Zhou, V. S. Zapf, and M. Lee, Electronic and magnetic phase diagrams of the Kitaev quantum spin liquid candidate  $\text{Na}_2\text{Co}_2\text{TeO}_6$ , *Phys. Rev. B* **108**, 064421 (2023).
- [45] C. Balz, L. Janssen, P. Lampen-Kelley, A. Banerjee, Y. H. Liu, J. Q. Yan, D. G. Mandrus, M. Vojta, and S. E. Nagler, Field-induced intermediate ordered phase and anisotropic interlayer interactions in  $\alpha\text{-RuCl}_3$ , *Phys. Rev. B* **103**, 174417 (2021).
- [46] P. Pilch, L. Peedu, A. K. Bera, S. M. Yusuf, U. Nagel, T. Rößm, and Z. Wang, Field- and polarization-dependent quantum spin dynamics in the honeycomb magnet  $\text{Na}_2\text{Co}_2\text{TeO}_6$ : Magnetic excitations and continuum, *Phys. Rev. B* **108**, L140406 (2023).
- [47] J. Wang and Z.-X. Liu, Effect of ring-exchange interactions in the extended Kitaev honeycomb model, *Phys. Rev. B* **108**, 014437 (2023).
- [48] W. Yao, K. Iida, K. Kamazawa, and Y. Li, Excitations in the ordered and paramagnetic states of honeycomb magnet  $\text{Na}_2\text{Co}_2\text{TeO}_6$ , *Phys. Rev. Lett.* **129**, 147202 (2022).
- [49] A. K. Bera, S. M. Yusuf, F. Orlandi, and P. Manuel, Magnetic phase diagram of the quasi-2D honeycomb antiferromagnet  $\text{Na}_2\text{Co}_2\text{TeO}_6$  single crystal, STFC ISIS Neutron and Muon Source (2020), <https://doi.org/10.5286/ISIS.E.RB2010435-1>; A. K. Bera, S. M. Yusuf, F. Orlandi and P. Manuel, Magnetic phase diagram of the quasi-2D honeycomb antiferromagnet  $\text{Na}_2\text{Co}_2\text{TeO}_6$ , STFC ISIS Neutron and Muon Source (2019), <https://doi.org/10.5286/ISIS.E.101136877>.